Simulating Flow Changes Due to Marine Hydrokinetic Energy Devices: SNL-EFDC Model Validation

Prepared by:							
Seth Shill							
Faculty Advisor:							
Professor Mary Cardenas, Harvey Mudd College							
Research Collaborator:							
Scott C. James, PhD., E ^x ponent, Inc.							

July 27, 2013

Abstract

Marine hydrokinetic energy (MHK) devices generate electricity by removing energy from tidal currents. In the process, MHK devices create wakes. The structure and dissipation of these wakes have been studied yet little research has characterized the large-scale hydrodynamics and environmental effects due to MHK devices. The research objective of this study was to validate MHK-specific turbulence models. The computational fluid dynamics model SNL-EFDC was used to simulate three experimental flume studies; these models are intended for use in parameter estimation. The results of this study present modified experimental models capable of predicting correct steady-state inlet velocities. For each model, predicted velocity deficits matched physical expectations.

Introduction

Marine hydrokinetic energy (MHK) devices generate electricity by removing energy from tidal currents. These devices can be found in many different forms and may be placed wherever there is a tidal flow

(see figure 1 depicting a hypothetical tidal turbine farm). Demonstration MHK projects have already been built in the U.S., such as the TidGen tidal turbines placed in Cobscook Bay, Maine. To generate a substantial proportion of electricity, MHK devices must be implemented in farms or arrays. This presents challenges to MHK energy generation; specifically, the wake created by MHK devices is significant enough to force the arrangement of arrays into suboptimal positions, affecting the downstream spacing and density of turbines and thus total power available. Additionally, volumetric flows and tidal ranges can be altered when large



Figure 1: Artist's depiction of a tidal current turbine array, picture courtesy of The Guardian [19].

numbers of tidal current devices occupy a spatially-constrained area. These effects have significant consequences on local marine life.⁴ Accurate hydrodynamic and environmental modeling can provide advantages towards optimizing power efficiency while minimizing these environmental costs.



Past research using both small-scale actuator disk experiments and scaled turbines has provided insight into the wake structure and its

y Dept. Spends \$10 Million on Water Turbine to Power 25 ervative Policy News Blog from The Heritage Foundation. The eb. 01 Aug. 2013.

erimental analysis of the flow field around horizontal axis tidal sh disk rotor simulators, Ocean Engineering, 37 (2010) 218-227. covery of MHK turbines, ORNL/TM-2012 (2012).

Ite, In-stream tidal energy potential of Puget Sound, Washington,

Proceedings of the Institution of Mechanical Engineers, Part A: Journal of Power and Energy, 223 (2009) 571-587.

ale three-blade at the Saint oratory (SAFL) tesy of [20]. dissipation downstream of the MHK-device.^{5,6,7,8,9,10} These studies found altered tidal elevations at the coastline and within the immediate area surrounding these devices. However, more research is required to develop accurate simulation tools that quantify and visualize the influence MHK devices have on flow characteristics, sediment transport, and water quality.

This research calibrates wake parameters by comparing predicted model velocity deficits to experimentally-determined velocity deficits. The experimental velocities were determined from three scaled models of single actuator disks (Saint Anthony National Falls Laboratory [SAFL]¹¹, IFREMER¹², and Chilworth¹³ flumes) and one scaled-model of three actuator disks (Chilworth¹⁴ flume). Neary et. al. examined the wake flow recovery downstream of a 1:10 scale model, axial-flow hydrokinetic turbine in the SAFL flume (depicted in Figure 2), while Myers et. al. observed near wake properties of marine horizontal-axis current turbines using the IFREMER flume. Myers and Bahaj (2010) analyzed the flow field around horizontal axis tidal turbines in the Chilworth single actuator disk experiment. Finally, the Chilworth three actuator disks model (depicted in Figure 3) investigated inter-array wake properties in tidal turbine arrays. Computational fluid dynamics code (EFDC) modified with a Sandia National

⁵ A.S. Bahaj, A.F. Molland, J.R. Chaplin, W.M.J. Batten, Power and thrust measurements of marine current turbines under various hydrodynamic flow conditions in a cavitation tunnel and a towing tank, Renewable Energy, 32 (2007) 407-426.

⁶ L.E. Myers, A.S. Bahaj, Experimental analysis of the flow field around horizontal axis tidal turbines by use of scale mesh disk rotor simulators, Ocean Engineering, 37 (2010) 218-227.

⁷ X. Sun, Numerical and experimental investigation of tidal current energy extraction, in: School of Engineering, University of Edinburgh, Edinburgh, UK, 2008, pp. 212.

⁸ T. O'Doherty, A. Mason-Jones, D.M. O'Doherty, C.B. Byrne, I. Owen, Y.X. Wang, Experimental and computational analysis of a model horizontal axis tidal turbine, in: 8th European Wave and Tidal Energy Conference, Uppsala, Sweden, 2009, pp. 833-841.

⁹ V.S. Neary, B. Gunawan, C. Hill, L.P. Chamorro, Wake flow recovery downstream of a 1:10 scale axial flow hydrokinetic turbine measured with pulse-coherent acoustic Doppler profiler (PC-ADP), ORNL/TML-2012 (2012)

¹⁰ L.E. Myers, A.S. Bahaj, Near wake properties of horizontal axis marine current turbines, in: Proceedings of the 8th European Wave and Tidal Energy Conference, Uppsala, Sweden, 2009, pp. 558-565

¹¹ V.S. Neary, B. Gunawan, C. Hill, L.P. Chamorro, Wake flow recovery downstream of a 1:10 scale axial flow hydrokinetic turbine measured with pulse-coherent acoustic Doppler profiler (PC-ADP), ORNL/TML-2012 (2012).

¹² L.E. Myers, A.S. Bahaj, Near wake properties of horizontal axis marine current turbines, in: Proceedings of the 8th European Wave and Tidal Energy Conference, Uppsala, Sweden, 2009, pp. 558-565.

¹³ L.E. Myers, A.S. Bahaj, Experimental analysis of the flow field around horizontal axis tidal turbines by use of scale mesh disk rotor simulators, Ocean Engineering, 37 (2010) 218-227.

¹⁴ L.E. Myers, B. Keogh, A.S. Bahaj, Experimental investigation of inter-array wake properties in early tidal turbine arrays, in: OCEANS 2011, 2011, pp. 1-8.

Laboratories MHK module (SNL-EFDC) was used to predict flow variables, sediment dynamics, and water quality surrounding MHK devices in flumes¹⁵

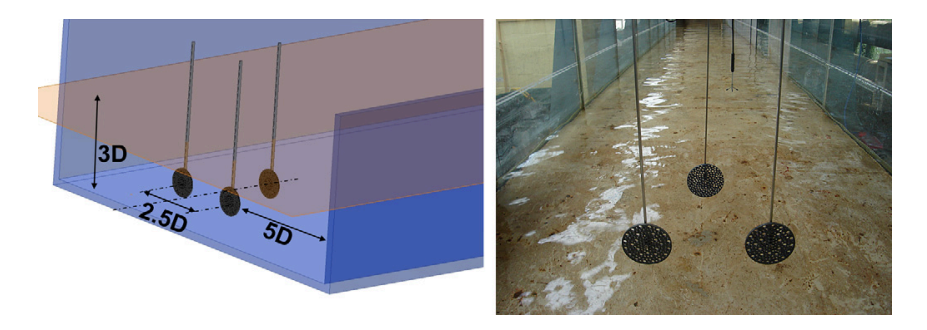


Figure 3: Arrangement of the 3-disk array in the Chilworth circulating flume, courtesy of [21].

Objectives

The objective of this research was to validate MHK-specific turbulence models. Specifically, model parameters β_p , β_d , C_{e4} , C_{pb} , and α_{md} are calibrated against three experimental flume studies using computational fluid dynamics (CFD) code, SNL-EFDC, to simulate flow conditions (see Overall Approach for where these model parameters come from).

Overall Approach

Model Framework

This research calibrates existing models of laboratory flume experiments using ocean circulation computational fluid dynamics code (CFD) and a nonlinear parameter optimization wrapper program. The CFD model applied, SNL-EFDC, was developed by the U.S. Environmental Protection Agency and modified with an MHK module by Sandia National Laboratories to model fluid flow, sediment transport, and water quality. SNL-EFDC uses hydrostatic, free surface, Reynolds Averaged Navier-Stokes equations with Mellor-Yamada turbulence closure to solve for numerical solutions using parameter inputs.

Marine Hydrokinetic Simulation Module

The MHK simulation module simulates "removal of momentum from model cells."¹⁶ Turbulent kinetic energy and its dissipation rate were predicted using a canopy model adopted from wind-energy research.¹⁷ Equations for rate of momentum reduction, net change in turbulent kinetic energy, and

¹⁵ S.C. James, E. Seetho, C. Jones, J. Roberts, Simulating environmental changes due to marine hydrokinetic energy installations, in: OCEANS 2010, Seattle, WA, 2010, pp. 1-10

¹⁶ S.C., James, E. Johnson, J. Barco, and J. D. Roberts, Simulating flow changes due to marine hydrokinetic energy devices: SNL-EFDC model validation, (2013) 3.

¹⁷ G.G. Katul, L. Mahrt, D. Poggi, C. Sanz, One- and two-equation models for canopy turbulence, Boundary-Layer Meteorology, 113 (2004) 81-109.

¹⁸ S.C., James, E. Johnson, J. Barco, and J. D. Roberts, Simulating flow changes due to marine hydrokinetic energy devices: SNL-EFDC model validation, (2013) 3.

Appendix A:

Figure 1 Location of actuator disk (red) in SAFL flume experiment.

Figure 2 Location of actuator disk (red) in IFREMER flume experiment.

Figure 3 Location of actuator disk (red) in Chilworth single disk flume experiment.

Figure 4 Location of actuator disk (red) in Chilworth array flume experiment.

Figure 5 Depth-averaged velocity field for steady-flow solution of SAFL simulation.

Figure 6 Depth-averaged velocity field for steady-flow solution of IFREMER simulation.

¹⁹ Carrell, Severin. "10MW Tidal Power Station Gets Scottish Government's Approval." *The Guardian*. The Guardian, 11 Mar. 2011. Web. 30 July 2013.

²⁰ V.S. Neary, B. Gunawan, C. Hill, L.P. Chamorro, Wake flow recovery downstream of a 1:10 scale axial flow hydrokinetic turbine measured with pulse-coherent acoustic Doppler profiler (PC-ADP), ORNL/TML-2012 (2012).

²¹L.E. Myers, A.S. Bahaj, An experimental investigation simulating flow effects in first generation marine current energy converter arrays, in: Renewable Energy, 37 (2012) 33.

increase in turbulent kinetic energy dissipation rate are represented as S_Q , S_k , and S_ϵ , and in equations 1-3:

$$\begin{split} S_{\varrho} &= -\frac{1}{2} C_{\mathrm{T}} A U^{2}, \\ S_{k} &= \frac{1}{2} C_{\mathrm{T}} A \left(\beta_{\mathrm{p}} U^{3} - \beta_{\mathrm{d}} U k \right), \\ S_{\varepsilon} &= C_{\varepsilon 4} \frac{\varepsilon}{k} S_{k}, \end{split}$$

where " C_T is the thrust coefficient, U is the flow speed (in m/s), A is the flow facing area of the turbine/blades and/or support structure (in m²), β_p is the fraction of mean flow kinetic energy converted to wake-generated energy, k is a nondimensional factor (m²/s²), β_d is the factor of k dissipated by conversion to turbine kinetic energy, ϵ is the kinetic energy dissipation rate (m²/s³), and $C_{\epsilon 4}$ is a closure constant." ¹⁸

Experimental Setup

Each experimental flume was modeled and analyzed. These simulations were designed to emulate laboratory conditions experienced by mock MHK devices. To match experimental setups, models with proper dimensions & flow conditions were created using the EFDC Explorer (EE) GUI. The EE GUI served as an interface to modify and visualize boundary conditions, flow conditions, and model parameters such as depth, surface elevation, and vegetation type at the cellular and multicellular level. Computational fluid dynamics (CFD) code SNL-EFDC was used to calculate and visualize velocities for a specific MHK device arrangement based on given input parameter values. These velocities were viewed as a heat plot in the EE GUI.

In addition, SNL-EFDC computes the velocity deficits based on the computed velocities occurring either downstream or upstream of the actuator disk(s). Velocity deficit is a non-dimensional number that can be characterized by equation 4,

Figure 7 Depth-averaged velocity field for steady-flow solution of Chilworth single disk simulation.

Figure 8 Depth-averaged velocity field for steady-flow solution of Chilworth array simulation.

$$U_{deficit} = 1 - \frac{U_w}{U_0}$$

where \boldsymbol{U}_w is the velocity of the wake generated by the disk, and \boldsymbol{U}_0 is the free stream velocity. For modeling physical conditions, velocity deficits are expected to always be positive and less than 1. Also, velocity deficits are expected to decrease over distance downstream as wake velocity returns closer to free stream velocity. These values can be viewed as time-referenced output from SNL-EFDC computations, and then analyzed according to expectations and physical meaning. With this information and analysis, the steady-flow model experiment is constructed.

Methods:

Steady-State Verification

SNL-EFDC simulated flow through each experimental model. For a given model, a single iteration of SNL-EFDC was run for a particular number of reference periods based on the model time step. The results were visually analyzed in EFDC Explorer (EE), a GUI that facilitates plotting of heat graphs for model parameters in addition to visualizing cell coordinates and dimensions. Velocity deficits were also analyzed for linearity, and accuracy in modeling physical conditions.

For each model, the correct inlet velocity (U) was determined based on the volumetric flow rate (Q) through each inlet cell. In general, the inlet velocity can be calculated as

$$U = \frac{(BC)Q}{wd}$$

where BC is the total number of inlet boundary cells, w is the width of the flume, and d is the depth of the flume. In models with non-uniform cell dimensions, the volumetric flow rate Q is scaled by an appropriate proportion factor for that model cell.

Development of New Models

The Chilworth single actuator disk, Chilworth 3 actuator disk, and SAFL models were modified to better depict experimental dimensions and parameters (see Table 1). SAFL was modified to have dimensions that would allow for centering the disk and correcting for the right width of the experimental flume. This was done in EFDC Explorer (EE) by generating a new Cartesian grid and $10 \times 10 cm^2$ cells. The cells making up the sidewalls of the flume were stretched to $10 \times 12.5 \ cm^2$ to fit the exact dimensions of the flume to 3 significant figures. Once the grid was composed, SNL-EFDC is applied to the model to simulate flow in all wet cells comprising the interior of the flume. Once steady flow was achieved in a simple flume model, actuator disks (simulating turbines) were added to the grid model. To accurately model the actuator disk resistance, a vegetation type that accurately simulates turbines was chosen. A steady-state flow solution was again obtained with the disk in place, and the minimum time to reach that state was also recorded.

The Chilworth single actuator disk model grid was resized to correct for flume width, depth, and correct disk diameter. Starting from a previously designed grid by Erick Johnson, flow model cells adjacent to land on the longer flume sidewalls were lengthened to $3.3 \times 8.55 \ cm^2$ from a uniform grid of $3.3 \times 3.0 \ cm^2$ cells. The procedure for disk placement by SAFL was then replicated for the Chilworth single disk model, and grid cell size remained the same dimensions as Erick Johnson's model for the horizontal cells aligning the actuator disk. Using three vertical cells, the actuator disk was constructed with a diameter of $0.099 \ m$ from $3.3 \times 3.3 \ cm^2$, approximately $0.001 \ m$ short of the actual dimension. Horizontal cells located at the j-value above or below the center disk were modified to $3.3 \times 2.55 \ cm^2$ to account for this deficit. A similar procedure to SAFL was followed to prepare the Chilworth single disk model for simulations using SNL-EFDC.

The Chilworth array model was built on the modified Chilworth single actuator disk grid since this model had proper center-width disk placement. Using three vertical cells, the center actuator disk was constructed with a diameter of 0.099m, approximately 0.001m short of the actual dimension. Horizontal cells located at the j-value above or below the center disk were modified to $3.3 \times 2.55 \ cm^2$ to account for this deficit. Cells located at the longer flume sidewalls were stretched to $3.3 \times 3.9 \ cm^2$ to reach the correct flume width. Two 100mm-diameter actuator disks were then placed at experimentally determined locations, 3 device diameters (D) upstream. The same procedure was followed as the SAFL and Chilworth single disk models for running PEST simulations.

Lastly, the vertical displacements of actuator disks within model layers were validated using experimental dimensions for each flume. Table 2 lists the dimensions of the MHK support structures and MHK device itself used to determine the bottom, center, and top layers of the MHK device. BOFFSUP is the offset of the support structure bottom from the flume bottom; BOFFMHK is the offset of the MHK device bottom from the flume bottom; TOFFSUP is the offset of the support structure top from the flume bottom; and TOFFMHK is the offset of the MHK device top from the flume bottom, while CTR, TOP, and BTM layers are the layers in which the center (nacelle), uppermost portion, and bottommost portion of the MHK device lay.

Experimen	Length	Width (m)	Depth (m)	Roughnes	Layers	Cells I	Cells J
t	(m)			S			
SAFL	15	2.75	1.155	0.002	12	29	150
IFREMER	18	4.00	2.0	0.004	16	112	25
Chilworth	21	1.35	0.5	0.075	10	212	41
Single Disk							
Chilworth	21	1.35	0.5	0.075	10	212	41
3 Disk							

Table 1 Experimental and model parameters for each of the four experiments. Experimental length, width, depth, and roughness were identical or nearly identical to model dimensions for SAFL & IFREMER experiments, and scaled for Chilworth models (actual model length was 7m long). Layers, Cells I, and Cells J are model parameters used for simulation purposes only. Layers represent the total number of model layers, and Cells I and Cells J represent the total number of cells in the I-and J-directions respectively.

<u>Parameters</u>	SAFL	IFREMER	3-disk	Single-disk
BOFFSUP	0	0.94	0	0
BOFFMHK	0.175	0.54	0.214	0.214
TOFFSUP	0.425	2	0.264	0.264
TOFFMHK	0.675	1.34	0.314	0.314
DEPTH	1.155	2	0.05	0.05
Layers	12	16	10	10
DCZ: Dimensional				
Layer Thickness	0.08333	0.0625	0.1	0.1
Layer thickness				
(m)	0.09624615	0.125	0.05	0.05
CTR Layer Exact	4.41576104602626	7.52	5.28	5.28
CTR Layer	5	8	6	6
TOP Layer Exact	7.01326754368876	10.72	6.28	6.28
TOP Layer	8	11	7	7
BTM Layer Exact	1.81825454836375	4.32	4.28	4.28
BTM Layer	2	5	5	5

Table 2 Turbine/Disk and support structure dimensions in meters and MHK-device center, bottom, and top location within model layers.

Simulation Results & Discussion

The inlet flow velocities for SAFL, IFREMER, Chilworth single disk, and Chilworth array flumes were determined as 0.398 m/s, 0.800 m/s, 0.220 m/s, and 0.212 m/s respectively using equation (5). These were verified by observing the flow velocity magnitudes near the flume inlet on the velocity heat plots generated by the EFDC Explorer GUI (see figures 5, 6, 7, and 8 in Appendix A).

The closeness in match between physical reality and model velocities were also validated visually and by observing the calculated velocity deficits at different device diameters downstream. Generally, slower velocities directly downstream of the actuator disk and within the width of the device are expected, with higher velocities just outside the width of the device. In addition, the velocity deficit should decrease at greater device diameters downstream as momentum diffuses throughout the model cells; that is, flow velocities increase in slower model cells to conserve kinetic energy. All these conditions were met for the SAFL and IFREMER experiments. Correct velocity deficits for Chilworth experiments were not obtained since we could not verify modeled actuator disk displacements for measuring flow velocities downstream.

Conclusion

Rebuilt models for SAFL, IFREMER, and Chilworth experiments improved model accuracy while maintaining flow stability. The actuator disk in the SAFL experiment model was centered, and correct flume roughness and turbine thrust coefficient (C_T) were applied to the model to obtain accurate inlet and flow velocities; in addition, the correct flume roughness was applied to the IFREMER model and again accurate inlet and flow velocities were obtained. Lastly, both Chilworth models were modified to

correct flume dimensions, roughness, and actuator disk placement. However, steady-flow solutions with realistic velocity deficits for the Chilworth experiments have yet to be obtained. Overall, all models were modified to better match experimental conditions.

Future Work

Future work would include better techniques to analyze optimized parameters using sensitivity analysis tools such as SENSAN, a plug-in program to PEST, as well as additional modifications to model cell grids to better optimize the balance between grid resolution and model accuracy. Specifically, the Chilworth grid would benefit in having a fewer number of model cells, implying a larger cell sizes. This would ensure greater flow stability by minimizing the influence of turbulent shear strain between grid cells.

In addition, further model simulations implementing various values of eddy diffusivity (α_{md}) are necessary to better understand the interaction between α_{md} and model parameters β_d , β_p , $C_{\epsilon 4}$, and C_{pb} . This could be done using parameter estimation software in order to arrive at best-fit correlation parameters describing α_{md} in relation to model parameters.

Acknowledgements

I would like to thank my advisors, Prof. Mary Cardenas and James C. Scott, Ph.D., for their time and round-the-clock help towards gaining a deeper understanding on the inner workings of this project. In addition, I would like to thank Prof. Cardenas for prompting me to apply for this wonderful research opportunity.

I would also like to thank Willie Drake of the computing and information services department for helping me with any software and/or hardware issues along the way.

Lastly, I want to thank the HMC Center for Environmental Studies for the funding and support of this project.

Citations